ACCSCIENCE PUBLISHING

Asian Journal of Water, Environment and Pollution. Vol. 22, No. 5 (2025), pp. 214-230.
doi: 10.36922/AJWEP025210162

ORIGINAL RESEARCH ARTICLE

Rheological optimization and diffusion modeling of fly ash–coal gangue composite slurries

Zhu Liu[1], Shupeng Wen[1], Jian Wang[2], Xiao Wang[2], Yang Yang[3], Zhongquan Liu[3],and Linqiang Mao[4]*

[1]Department of Mineral Engineering, 113 Team, Guizhou Coalfield Geology Bureau, Guiyang, Guizhou, China
[2]Department of Mineral Engineering, Guizhou Coalfield Geology Bureau, Guiyang, Guizhou, China
[3]Guizhou Qiandi Jingkai Technology Co., Ltd, Guiyang, Guizhou, China
[4]Department of Environmental Engineering, School of Environmental Science and Technology, Changzhou University, Changzhou, Jiangsu, China
***Corresponding author:** Linqiang Mao (maolq@cczu.edu.cn)

Received: May 20, 2025; Revised: July 10, 2025; Accepted: July 17, 2025; Published online: August 6, 2025

Abstract: The separation of overburden strata in coal mining directly affects surface subsidence, the ecological environment, and mining safety. Backfilling technology is currently the primary solution to address these issues. This study examines the rheological performance of a coal gangue and fly ash mixed slurry as a filling material under different raw material proportions and injection pressures, and predicts its diffusion distance using a theoretical model. Orthogonal experiments were conducted to evaluate the influences of solid volume concentration, coal gangue particle size, and fly ash-to-coal gangue mass ratio on the density, viscosity, and water bleeding rate of the slurry. Results demonstrated that solid volume concentration had the most significant influence on density and viscosity, followed by coal gangue proportion and particle size. Increasing coal gangue content elevated density and viscosity due to higher interparticle friction, while finer particles reduced viscosity by 30–40%. The introduction of a polycarboxylate superplasticizer achieved a 45% viscosity reduction with an optimal dosage of 0.3 wt%, by dispersing particles and enhancing the availability of free water compared to sulfamic acid. Injection pressure accelerated water bleeding rates by 20–35%, while finer coal gangue particles prolonged bleeding time. A power-law fluid fracture grouting diffusion model predicted that higher injection pressures (0.1–0.4 MPa) and fracture widths (0.4–1.0 mm) linearly increased diffusion distance, whereas steeper fracture angles (5–20°) enhanced the spread range. This study provides a broad perspective for designing cost-effective, environmentally stable grouting systems using coal-based waste, balancing injectability and long-term performance in mining applications.

Keywords: Overburden separation; Injection in separated-bed technology; Coal gangue; Fly ash

1. Introduction

The overburden separation space injection technique refers to a method that involves sealing the separated strata space above the water-conducting fracture zone and subsequently injecting grouting materials under high pressure to minimize the subsidence of overlying rock layers, prevent water infiltration into the separated strata, and inhibit stratum closure (Figure 1).[1] This technique aims to reduce ground subsidence and mitigate hazards caused by water accumulation in the separated strata. By effectively addressing mining-induced ground subsidence, reducing the surface accumulation of industrial waste, and preventing water-related stratum hazards, this technique is beneficial for coal mine structural safety and environmental conservation.[2] It has

demonstrated significant effectiveness and economic benefits in subsidence control across multiple mining areas in China.[2]

The primary objectives of strata separation injection are to mitigate ground subsidence, prevent water-related hazards in separated strata, and facilitate the disposal of mining solid waste. The ideal injection slurry should exhibit low viscosity and high fluidity to ensure effective diffusion to distant areas from the injection station.[3] Moreover, the slurries should have a low water bleeding rate to avoid pipeline clogging during prolonged grouting operations. The slurries must be environmentally safe, ensuring non-toxicity and minimal environmental impact to protect both geological formations and human health.

The key performance indicators for strata separation injection slurries include density, water bleeding characteristics, and viscosity.[4] In addition, the cost-effectiveness of materials must be taken into consideration during the raw material selection process. Fly ash has been proven to be the dominant material in mining areas for strata separation injection due to its low cost and accessibility, while its increasing demand – driven by the expanding application of diverse technologies – has led to shortages in some regions.[5] Consequently, coal gangue – a prevalent solid waste in coal mining areas – is being explored as a potential alternative raw material for injection slurries.

Critical challenges include determining the optimal grinding particle size for coal gangue to balance economic feasibility and slurry performance.[6] Although extensive research and engineering practices have focused on preparing slurries with fly ash, the development of injection slurries using coal gangue without cementitious materials remains limited, and diffusion modeling for such suspensions in fractured strata lacks experimental validation.[7,8] Specifically, studies on the fluid properties of slurries prepared from fly ash and coal gangue under injection pressure are relatively scarce. This gap underscores the need for systematic research to evaluate the compatibility, rheology, and long-term stability of such complex systems in practical injection applications.

This study investigates the rheological performance of coal gangue and fly ash mixed slurry as a filling material through orthogonal experiments. The evaluated performance parameters include water bleeding characteristics, density, and viscosity. Three independent factors – solid volume concentrations (e.g., 50%, 60%, and 70%), coal gangue particle sizes (e.g., 50, 100, and 150 mesh), and fly ash-to-coal gangue mass ratios (e.g., 7:3 and 3:7) —were systematically examined to analyze their effects on slurry properties. To improve viscosity, two types of superplasticizers – polycarboxylate and sulfamic acid – were analyzed for their role in reducing viscosity. Finally, the influence of injection pressure on the water bleeding rate of the slurry was analyzed to simulate practical injection conditions. This study provides valuable insights into the preparation and injection of fly ash–coal gangue mixed slurry.

2. Materials and methods

2.1. Raw materials

The chemical compositions and component contents of fly ash and coal gangue used in this study were analyzed using an X-ray fluorescence spectrometer (S8 Tiger, Bruker, Germany) and an X-ray diffraction system (D8, Bruker, Germany). The results revealed that coal gangue was predominantly composed of silicon dioxide, aluminum oxide, titanium dioxide, and ferric oxide, while fly ash primarily consists of silicon dioxide and ferric oxide (Table 1 and Figure 2). Fly ash is typically obtained by collecting fine residues from ground coal combustion and has a similar geological origin to coal gangue. Apart from differences in component proportions, the two raw materials share similar major crystalline phases, including quartz, hematite, and anhydrite. Elemental analysis did not detect high concentrations of heavy metals in fly ash or coal gangue, indicating their environmental safety for injection into the separated strata space.

Figure 3 illustrates the results of thermogravimetric-differential scanning calorimetry analysis of coal gangue and fly ash. The mass of coal gangue and fly ash declined by 6 wt% and 4 wt%, respectively, after heating to 400°C. This mass loss is typically attributed to the evaporation of water and the decomposition of organic matter. As the temperature further increased to 900°C, the mass continued to decrease due to the decomposition of carbonates and sulfates.

2.2. Orthogonal experimental design

A mixed-level L18 ($3^2 \times 5^1$) orthogonal array was adopted to systematically evaluate the main effects of the selected factors (factor A: solid volume concentration, factor B: coal gangue particle size, and factor C: fly ash-to-coal gangue mass ratio) on slurry properties. While orthogonal designs inherently assume minimal interaction effects to efficiently screen main factors, potential interactions were statistically assessed post-experiment using one-way analysis of variance

(Statistical Package for Social Sciences [SPSS], IBM, United States of America).

The initial assumption of negligible interactions was justified based on: (i) the primary objective of identifying dominant main effects influencing rheology; (ii) the established precedent in similar rheological studies of particulate suspensions using orthogonal arrays for factor screening; and (iii) subsequent statistical analysis confirming the overwhelming significance of main effects ($p<0.01$ for all factors across responses) and the absence of statistically significant two-way interactions ($p>0.05$) detected in our dataset. This approach provided an efficient framework for identifying the most influential parameters controlling slurry behavior. The orthogonal experimental design is presented in Table 2.

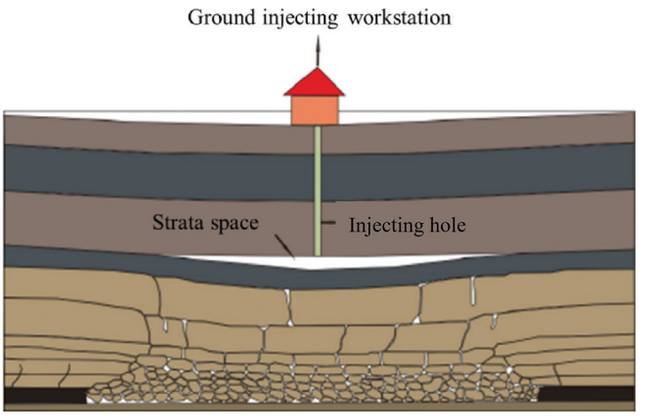

Figure 1. Schematic diagram of the injection process in separated-bed grouting

The solid volume concentration of grouting slurries is typically set between 50% and 80%.[9,10] Accordingly, this study selected three volume concentrations: 50%, 60%, and 70%. Larger coal gangue particle sizes reduce grinding costs, while excessively coarse particles may compromise slurry properties and increase injection costs. To analyze the influence of particle size on slurry performance, coal gangue was ground to three particle sizes: 50, 100, and 150 meshes. In addition, five fly ash-to-coal gangue mass ratios were selected: 7:3, 6:4, 5:5, 4:6, and 3:7.

2.3. Experimental procedure

The coal gangue was crushed using a grinder and sieved through 50, 100, and 150 mesh screens. Fly ash and coal gangue were weighed according to the predetermined mass ratios and transferred to a temperature-controlled mixing vessel maintained at 25 ± 2°C. Deionized water

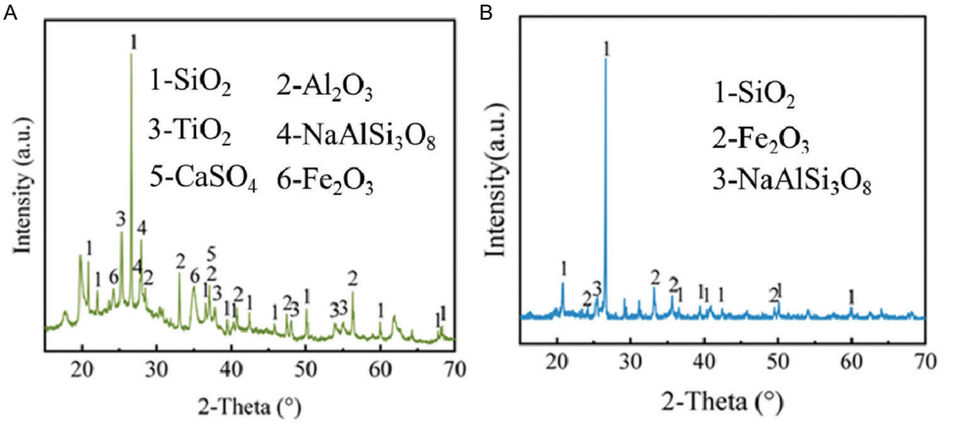

Figure 2. X-ray diffraction patterns: (A): Coal gangue, and (B) Fly ash.
Abbreviations: Al_2O_3: Aluminum oxide; $CaSO_4$: Calcium sulfate; Fe_2O_3: Ferric oxide; $NaAlSi_3O_8$: Sodium aluminum silicate; SiO_2: Silicon dioxide; TiO_2: Titanium dioxide

Table 1. Results of X-ray fluorescence analysis for coal gangue and fly ash

Compounds	SiO_2	Al_2O_3	CaO	Fe_2O_3	TiO_2	MgO	P_2O_5	Na_2O	K_2O	LOI[a]
Coal gangue	50.63	17.31	4.24	7.64	3.36	1.42	1.24	3.31	2.47	8.38
Fly ash	62.31	22.41	3.11	6.04	1.12	0.08	0.14	1.53	1.21	2.05

Note: [a]Mass loss of the sample upon heating to 950°C.
Abbreviations: Al_2O_3: Aluminum oxide; CaO: Calcium oxide; Fe_2O_3: Ferric oxide; K_2O: Potassium oxide; LOI: Loss of ignition; MgO: Magnesium oxide; Na_2O: Sodium oxide; P_2O_5: Phosphorus pentoxide; SiO_2: Silicon dioxide; TiO_2: Titanium dioxide.

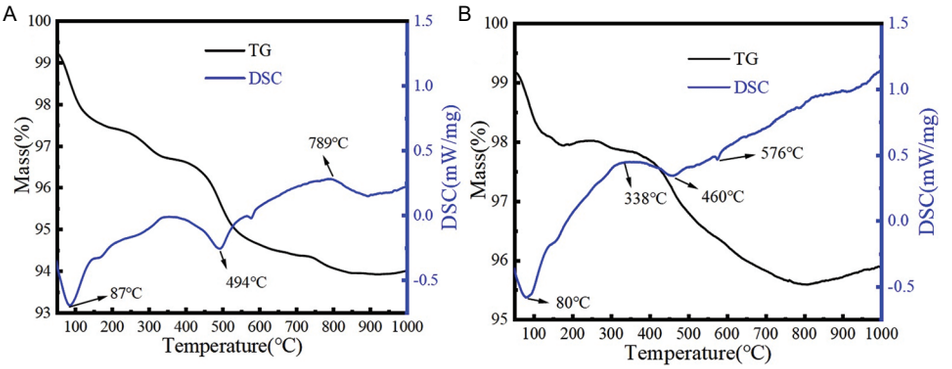

Figure 3. Thermogravimetry-differential scanning calorimetry analysis: (A) Coal gangue and (B) fly ash
Abbreviations: DSC: Differential scanning calorimetry analysis; TG: Thermogravimetry.

Table 2. Factors and levels used in the orthogonal experimental design

Level	Factor A: Solid volume concentration (%)	Factor B: Coal gangue particle size (mesh)	Factor C: Fly ash-to-coal gangue mass ratio
1	50	50	7:3
2	60	100	6:4
3	70	150	5:5
4	-	-	4:6
5	-	-	3:7

(25 ± 2°C) was gradually added while mixing at 300 ± 50 rpm using a digital overhead stirrer equipped with a four-blade propeller (diameter: 50 mm) (Mixing continued for 5 ± 0.5 min after complete water addition to ensure homogeneity). The slurry was immediately transferred to a 100 mL graduated cylinder maintained at 25 ± 2°C for density measurement and subsequent tests. For viscometry, 360 mL slurry samples were prepared under identical mixing conditions and tested within 2 min of preparation using a temperature-controlled (25 ± 0.5°C) rotational viscometer.

2.4. Reducing viscosity by superplasticizers

A slurry with a solid volume concentration of 60% was prepared and placed in 100 mL graduated cylinders for water bleeding experiments. Subsequently, 0.1 wt% of superplasticizer was added to each of these two slurries to conduct water bleeding tests. A mixture with a fly ash-to-coal gangue mass ratio of 3:7 and a solid volume concentration of 60% was selected as the representative sample to analyze the effect of superplasticizers on viscosity. Two types of superplasticizers – polycarboxylate and sulfamic acid – were selected and comparatively analyzed. To meet the operational requirements of the viscometer, 220 mL of slurry was prepared in a beaker, and viscosity tests were performed by adding superplasticizer dosages of 0.01, 0.03, 0.05, 0.1, 0.15, 0.2, 0.25, and 0.3 wt%.

2.5. Water bleeding rate of mixed slurries under injection pressure

The slurry was prepared with a solid concentration of 70%. Coal gangue particles of three sizes—50, 100, and 150 mesh—were selected. The fly ash-to-coal gangue mass ratio was controlled at 7:3, 6:4, 5:5, 4:6, and 3:7. Water bleeding tests were conducted under applied pressures of 0.1, 0.2, 0.3, and 0.4 MPa. The experiments examined the effects of coal gangue particle size, material ratio, and pressure on the water bleeding rate of the slurry.

The slurry was manually stirred with a glass rod directly in the pressure vessel. Approximately 200 mL of slurry was prepared for each ratio, and pressure was applied to the vessel immediately after mixing. A stopwatch was used to record the bleeding volume. Due to the rapid bleeding observed during the 1st min, measurements were taken every 5–10 s. After the 1st min, bleeding slowed, and measurements were recorded at 1-min intervals until no further bleeding occurred. The total bleeding volume was recorded to calculate the final water bleeding rate of the slurry.

3. Results and discussion

3.1. Effect of composition on rheological properties

3.1.1. Influence on slurry density

In this study, the three selected factors were assumed to have no interaction effects. A mixed-level L18 ($3^2 \times 5^1$) orthogonal array was adopted, involving

18 experimental trials to prepare slurries. The density, viscosity, and water bleeding rate of the slurries were measured, and the results are summarized in Table 3. Statistical analysis of the orthogonal experimental data was performed using SPSS software.

The *p*-value reflects the degree of influence of each factor on the response variables: $p<0.01$ indicates an extremely significant difference, a *p*-value between 0.01 and 0.05 denotes a significant difference, and $p>0.05$ suggests no significant difference.[9-11]

The analysis conducted in this study included significance testing and marginal means analysis. Significance testing was used to evaluate the isolated effect of individual factors on the parameters by calculating marginal means. Marginal means represent the average values of dependent variables after eliminating the influence of other factors, thereby isolating the contribution of a single factor.[12] In conventional analyses, changes in dependent variables typically result from the combined influence of multiple factors.

The *p*-values for factors A (solid volume concentration), B (coal gangue particle size), and C (fly ash-to-coal gangue mass ratio) were all below 0.01 (Table 4), indicating extremely significant differences. This finding demonstrates that all three factors had statistically significant effects on slurry density. However, factor C exhibited a relatively higher *p*-value, indicating a less pronounced impact on slurry density compared to factors A and B, which demonstrated equivalent levels of significance. The order of influence of the three factors on slurry density is as follows: Fly ash-to-coal gangue mass ratio > solid volume concentration > coal gangue particle size.[13]

The marginal means of each factor were utilized to examine their individual effects on slurry density. The variations in marginal means for each factor are illustrated in Figure 4. Solid volume concentration plays a critical role in increasing slurry density (Figure 4A).[14] As the volume concentration increased, the slurry became more compact, resulting in higher density. A near-linear inverse relationship was observed between coal gangue particle size and slurry density (Figure 4B). The density decreased from approximately 1.37 g/cm^3 to 1.25 g/cm^3 as particle size decreased, due to finer particles generating larger interstitial volumes within the slurry. These voids are filled with water, thereby reducing the volumetric proportion of coal gangue and, consequently, lowering the overall density.[15-18]

The fly ash-to-coal gangue mass ratio exhibited a quasi-linear positive correlation with density (Figure 4C). Higher proportions of coal gangue increased slurry density due to the inherently greater density of coal gangue powder compared to fly ash. At a constant slurry volume, a higher coal gangue content proportionally elevated the overall density.[19] Higher solid concentrations (60–70%) reduce water consumption by 20–30% compared to 50% slurries, thereby lowering pumping costs and minimizing the risk of groundwater contamination from bleed water. Retained injectability

Table 3. Orthogonal experimental results

Sample	A[a]	B[b]	C[c]	Slurry density (g/cm^3)	Viscosity (mPa·s)	Water bleeding rate (%)
1	1	1	1	1.21	4.25	0.34
2	1	1	2	1.34	5.10	0.40
3	1	2	3	1.45	5.30	0.38
4	1	2	4	1.17	6.10	0.37
5	1	3	5	1.12	4.20	0.34
6	1	3	1	1.22	5.10	0.32
7	2	1	2	1.60	12.50	0.26
8	2	1	3	1.52	9.50	0.32
9	2	2	4	1.34	5.60	0.38
10	2	2	5	1.17	5.10	0.34
11	2	3	1	1.25	5.70	0.35
12	2	3	2	1.29	5.30	0.31
13	3	1	3	1.35	10.40	0.32
14	3	1	4	1.30	11.50	0.31
15	3	2	5	1.40	9.10	0.26
16	3	2	1	1.50	10.20	0.24
17	3	3	2	1.38	7.40	0.31
18	3	3	3	1.37	8.10	0.32

Notes: [a]Solid volume concentration in the slurry; [b]coal gangue particle size; and [c]fly ash-to-coal gangue in the mixed slurry.

Table 4. Significance analysis of influencing factors on slurry density

Factor	Sum of squared deviations	DOF	Average variance	*F*-value	*p*-value
A	0.051	3	0.030	32.481	0.000
B	0.042	2	0.025	24.972	0.001
C	0.043	6	0.010	12.339	0.002
Deviation	0.016	7	0.002		
Sum	30.036	18			

Abbreviation: DOF: Degrees of freedom.

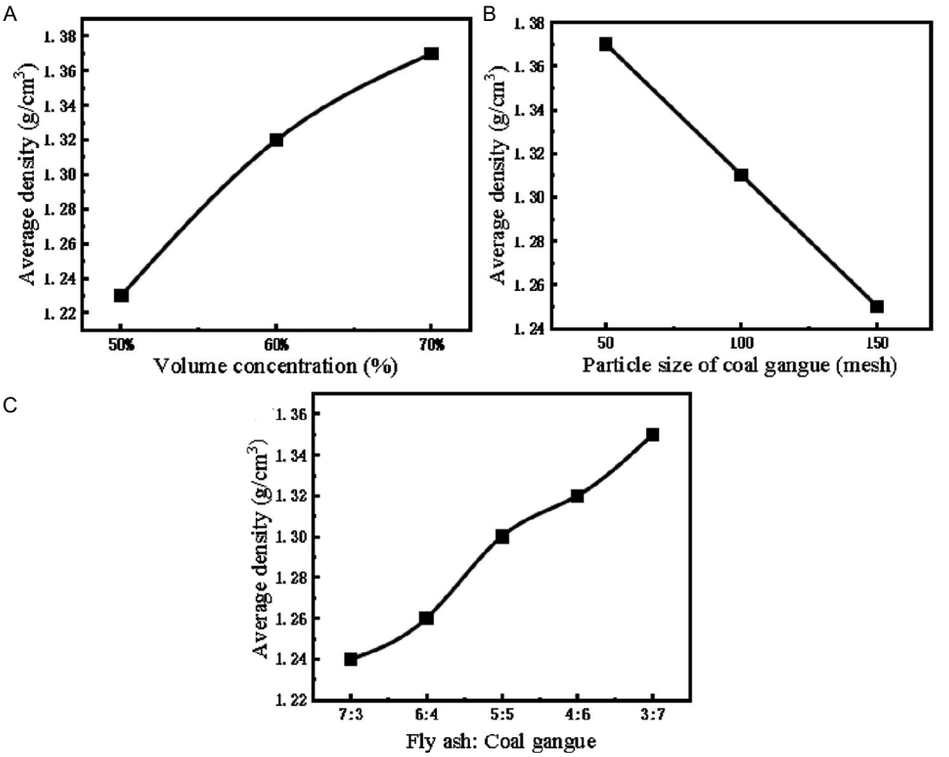

Figure 4. Influence of three factors on the estimated marginal mean of slurry density: (A) Solid volume concentration, (B) coal gangue particle size, and (C) fly ash-to-coal gangue mass ratio

at optimized viscosity ensures complete fracture filling with fewer boreholes, ultimately reducing drilling costs.

3.1.2. Influence on slurry viscosity

The influences of the three factors on slurry viscosity are presented in Table 5. The *p*-values for factors A, B, and C were all below 0.01, indicating extremely significant differences. This finding demonstrates that all three factors significantly affect slurry viscosity. Although factor C remained statistically significant, its influence on viscosity was less pronounced compared to factors A and B. The order of influence of the three factors on slurry viscosity is as follows: Solid volume concentration > coal gangue particle size > fly ash-to-coal gangue mass ratio.

The marginal means of each factor were employed to analyze the variations in slurry viscosity under the influence of individual factors, as illustrated in Figure 5. Solid volume concentration exhibited a highly significant effect on viscosity. Increasing solid concentration reduces particle spacing, altering their arrangement and interactions, which leads to higher viscosity.[19,20] A clear inverse relationship was observed between coal gangue particle size and slurry viscosity. As the particle size decreased from 50 mesh to 200 mesh, viscosity decreased from 9 to 5.5 mPa·s. This reduction is attributed to smaller particles having lower internal friction angles and reduced interparticle friction, which collectively reduce flow resistance.[21-23]

Table 5. Significance analysis of influencing factors on slurry viscosity

Factor	Sum of squared deviations	DOF	Average variance	F-value	*p*-value
A	42.833	2	20.432	17.333	0.001
B	32.375	3	17.685	12.163	0.002
C	51.147	6	12.113	8.812	0.003
Deviation	15.896	9	3.576		
Sum		17			

Abbreviation: DOF: Degrees of freedom.

The fly ash-to-coal gangue mass ratio showed an approximately linear correlation with viscosity. Increasing the coal gangue proportion raised the viscosity from 5 to 10.5 mPa·s. Fly ash particles are significantly finer than coal gangue particles; thus, higher coal gangue content hinders particle mobility and amplifies internal friction and viscosity.[24] Notably, viscosity increased gradually at mass ratios of 7:3 and

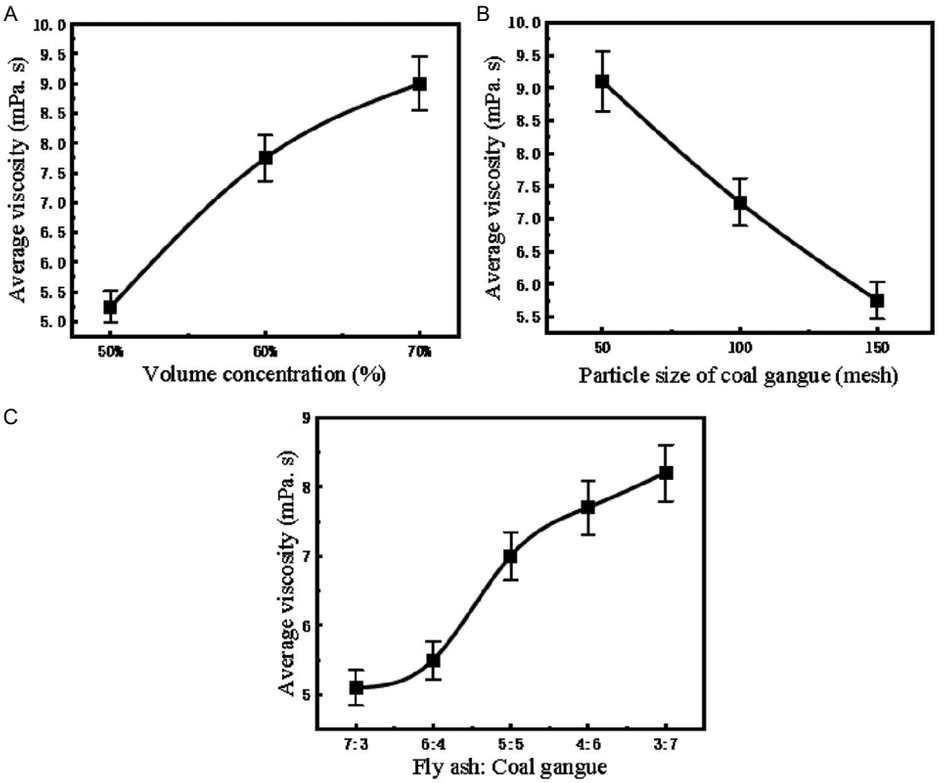

Figure 5. Influence of three factors on the estimated marginal mean of slurry viscosity: (A) Solid volume concentration, (B) coal gangue particle size, and (C) fly ash-to-coal gangue mass ratio

3:7, suggesting that excessive coal gangue promotes particle agglomeration, thereby accelerating viscosity buildup. Therefore, optimizing the fly ash-to-coal gangue mass ratio is crucial to balancing the viscosity and injectability of the slurry.

3.1.3. Influence on water bleeding rate

The test results for the influence of the three factors on the water bleeding rate are presented in Table 6. Factors A and C exhibited equivalent levels of significance ($p<0.01$), indicating extremely significant differences and confirming that both solid volume concentration and coal gangue mass proportion have a highly significant impact on slurry water bleeding rate.[24] In contrast, factor B showed a higher *p*-value (i.e., less statistical significance), indicating that its effect on the water bleeding rate was less pronounced compared to factors A and C. The order of influence of the three factors on the water bleeding rate is as follows: solid volume concentration = fly ash-to-coal gangue mass ratio > coal gangue particle size.

The marginal means of the three factors were utilized to examine their variations in the water bleeding rate (Figure 6). Solid volume concentration plays a key role in determining the water bleeding rate. As the volume concentration increased, the water bleeding rate decreased significantly, which is attributed to the higher proportion of solid particles relative to water during slurry preparation, thereby reducing bleed water.[25,26] A near-linear relationship was observed between volume concentration and water bleeding rate. When the concentration increased from 50% to 70%, the average water bleeding rate declined from 0.39 to approximately 0.29 (Figure 6A).

Coal gangue particle size exhibited minimal impact on the water bleeding rate. Although finer particles (e.g., 100 mesh) slightly reduced water bleeding compared to coarser particles (50 mesh), the difference was negligible (Figure 6B). Coal gangue particles, due to their high density, initially experience strong resistance to water flow.[27] However, as sedimentation progresses, the settling velocity decreases, resulting in similar water bleeding rates across different particle sizes over time.

As illustrated in Figure 6C, the mass ratio of fly ash to coal gangue exhibited an approximately linear relationship with the slurry water bleeding rate. As the proportion of coal gangue increased, the water bleeding rate decreased from 0.38 to approximately 0.28,

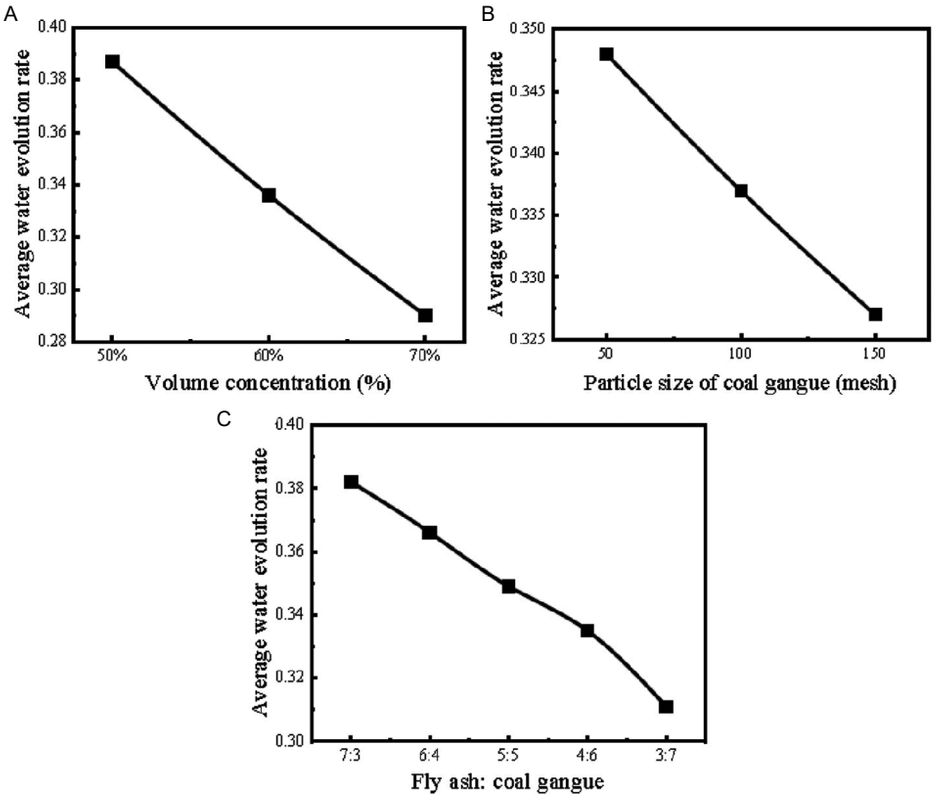

Figure 6. Influence of three factors on the estimated marginal mean of water bleeding rate: (A) Solid volume concentration, (B) coal gangue particle size, and (C) fly ash-to-coal gangue mass ratio

Table 6. Significance analysis of influencing factors on the water bleeding rate of slurry

Factor	Sum of squared deviations	DOF	Average variance	F-value	*p*-value
A	0.021	2	0.011	35.290	0.000
B	0.011	4	0.015	13.566	0.001
C	0.014	6	0.002	15.644	0.000
Deviation	0.003	8			
Sum	1.105	18			

Abbreviation: DOF: Degrees of freedom.

indicating that higher coal gangue content in slurry reduced water separation. Notably, when the mass ratio ranged from 7:3 to 4:6, the water bleeding rate declined gradually. However, when the fly ash-to-coal gangue mass ratio shifted from 4:6 to 3:7, the water bleeding rate declined significantly. This suggests that the variations in water bleeding at different stages were due to changes in particle packing density and interstitial water retention mechanisms at higher coal gangue proportions.[28,29] These findings align with the previous study by Du *et al.*,[17] which demonstrated that a higher solid volume concentration (60–70%) reduced bleeding by 20–40% (Figure 6A). However, unlike cemented tailings, fly ash—coal gangue slurries achieved stability without cement, thereby reducing costs.

This study suggests that replacing 40–70% of fly ash with coal gangue (mass ratio 6:4 to 3:7) can directly reduce raw material costs. Fly ash is priced at 20–50$ per ton in China, whereas coal gangue is a zero-cost industrial byproduct that only requires grinding. For a typical backfilling operation utilizing 100,000 tons of solids per year, substituting 50% of fly ash with coal gangue could result in annual savings of 0.75–2.25$ million. In addition, incorporating coal gangue at 40–70% mass ratio diverts 40,000–70,000 tons of waste per year from landfills for every 100,000 tons of backfill, thereby avoiding landfill disposal fees of 5–15$/ton and generating additional savings of $0.2–1.05 million annually. Moreover, this approach mitigates long-term environmental liabilities associated with coal gangue stockpiles.

3.2. Effect of superplasticizer on rheological properties

In practical engineering applications, slurry is typically transported through pipelines into grouting layers.[24,30]

Prolonged pipeline transportation can inevitably cause blockages, thereby hindering grouting operations. Therefore, higher slurry fluidity is advantageous for the injection process, and the water bleeding rate serves as an indicator of slurry stability.[30] A slower precipitation rate and lower water bleeding rate are desirable, as they enhance the long-term stability of the ground surface post-injection.[31]

This study investigated viscosity reduction by introducing various dosages of superplasticizer into the slurries to determine the optimal dosage. Both slurries were placed in 100 mL graduated cylinders, thoroughly stirred with a glass rod, and subjected to water bleeding rate tests. Subsequently, 0.1 wt% of superplasticizer–either polycarboxylate or sulfamic acid—was added to each slurry. Based on experimental results, polycarboxylate superplasticizer was identified as a more effective additive for significantly reducing viscosity compared to sulfamic acid. As a lipid-based, carbon-storing compound, polycarboxylate superplasticizer also exerts minimal environmental impact.[32]

As shown in Figure 7, the viscosity of both slurries generally decreased with increasing dosages of polycarboxylate superplasticizer and gradually reached a plateau. When the dosage reached 0.3 wt%, the viscosity remained stable. Notably, the viscosity of the fly ash–coal gangue slurry initially increased slightly but subsequently decreased and plateaued as the dosage continued to increase. This phenomenon is attributed to the chain-like molecular structure of polycarboxylate, which effectively disperses fly ash and coal gangue particles within the slurry, thereby reducing interparticle interactions.[27,28] These results confirm that polycarboxylate superplasticizer significantly reduces the viscosity of fly ash—coal gangue slurry.

The zeta potentials of fly ash—coal gangue slurry containing either sulfamic acid or polycarboxylate at mass fractions of 0–0.3 wt% were measured, as illustrated in Figure 8. Upon increasing the superplasticizer concentration to 0.01%, the surface potential of coal gangue increased from −14.9 mV to −12.04 mV, and further to −10.50 mV. This behavior is attributed to the adsorption of hydrophilic groups in polycarboxylate onto the surface of coal gangue, forming stable hydration films through interactions with water molecules. These films concurrently reduce the surface potentials of both raw materials, enhance particle wettability, diminish interparticle spacing by weakening electrostatic repulsion, and thin the hydration film around particles–collectively increasing the free water content and improving slurry fluidity.[33,34]

Although higher superplasticizer concentrations (>0.1%) exhibited limited efficacy in further reducing zeta potential, their extended polymer chains sterically stabilized the system by uniformly dispersing particles within the slurry matrix. This enhances colloidal stability through combined electrostatic and steric mechanisms.[15,21] These hydration films simultaneously reduce the surface potential of both raw materials (Figure 8), enhance particle wettability, and provide steric repulsion via extended polymer chains.[15]

Sulfamic acid is widely used to control water bleeding in cementitious systems due to its low cost, high dosage tolerance, and compatibility with cement matrices.[30] However, its application is often limited by poor compatibility with supplementary cementitious materials–such as fly ash or steel slag—which may result in bleeding or segregation due to inconsistent particle—fluid interactions.[33] In contrast, polycarboxylate superplasticizer—a lipid-based,

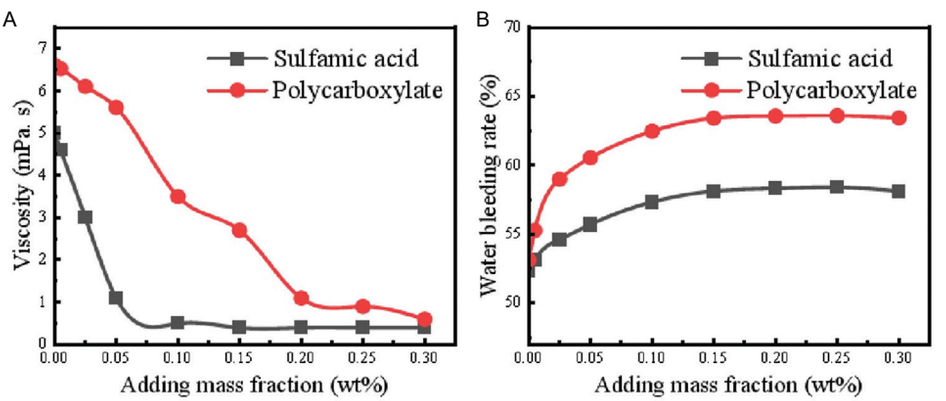

Figure 7. Influence of sulfamic acid and polycarboxylate superplasticizer on: (A) slurry viscosity and (B) water bleeding rate

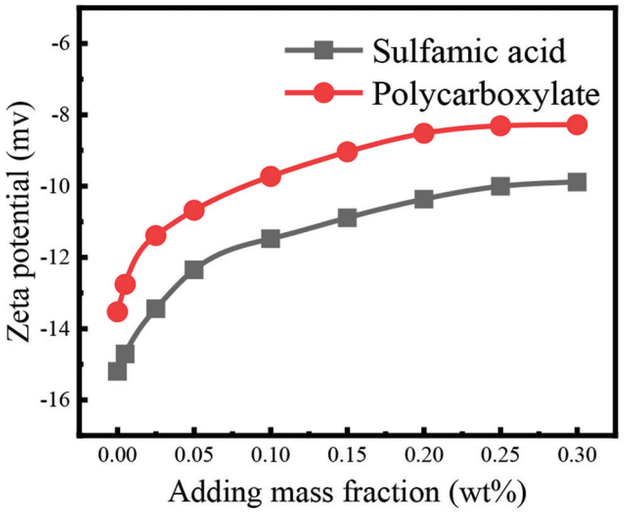

Figure 8. Effect of sulfamic acid and polycarboxylate superplasticizer on the zeta potential of mixed slurries

carbon-storing polymeric compound—exhibits superior environmental compatibility and minimal ecological impact.[31] Its molecular structure promotes efficient particle dispersion and robust fluidity retention, making it a more viable option for reducing viscosity in backfill grouts while ensuring long-term stability.

3.3. Effect of injection pressure on rheological properties

Figure 9 illustrates the viscosity of the fly ash–coal gangue mixing slurry at different fly ash-to-coal gangue mass ratios under various injection pressures. An increase in both injection pressure and fly ash proportion in the slurry resulted in higher viscosity. Since the particle size of fly ash is smaller than that of coal gangue, a decrease in coal gangue particle size resulted in a significant increase in slurry viscosity. Increasing the fly ash content not only raised the viscosity but also reduced injectability, thereby negatively impacting grouting and filling operations in coal mine goaf foundations. This effect is attributed to the fine particle size and high water absorption capacity of fly ash.

When 150-mesh coal gangue was incorporated, a large amount of water in the slurry was absorbed by the coal gangue particles, substantially reducing the free water content. This reduction in free water severely weakened the lubricating effect between particles, ultimately increasing the viscosity and deteriorating injectability. At elevated injection pressures, slurry viscosity increased as shear stress rose. This occurred because the aligned arrangement of finer fly ash and coal gangue particles under shear temporarily reduced internal friction, thereby improving fluidity. However, this effect is often limited due to the inherent high water absorption and fine particle characteristics of fly ash.

Figure 10 shows the variation curves of the water bleeding rate of slurries with a 70% solid volume concentration under different pressure conditions. The results demonstrated that higher pressure accelerated water bleeding and shortened the time required to complete the process, exhibiting an approximately linear relationship between bleeding rate and pressure. Finer coal gangue particle sizes reduced the water bleeding rate and prolonged the precipitation process of the slurry.

As the fly ash-to-coal gangue mass ratio decreased, the time required to complete bleeding increased, suggesting that a higher coal gangue content in the mixture lowers the bleeding rate. This effect is attributed to the larger interparticle voids in coarse coal gangue particles, which must be filled by fly ash or water.[22] Variations in mass ratios resulted in differences in void filling by water and fly ash, thereby influencing the bleeding rate. Finer coal gangue particle sizes further suppressed bleeding by reducing interparticle voids. For slurries containing 50-mesh coal gangue, the water bleeding rate ranged from 50% to 70%. At 100 mesh, the bleeding rate increased to 55–75%, while at 150 mesh, it stabilized around 55–65%. Overall, no distinct correlation was observed between coal gangue particle size and bleeding rate under pressure conditions, suggesting that particle size does not directly determine the bleeding behavior of slurry under such conditions.

3.4. Prediction of slurry diffusion distance using the power-law fluid fracture grouting diffusion model

The power-law fluid fracture grouting diffusion model was used to analyze the behavior of slurry diffusion in inclined fractures under various influencing factors, aiming to determine the optimal injection pressure, spacing, and strata layout for horizontal branch holes.[22] This model provides valuable insights into the fundamental relationships between injection parameters (e.g., pressure, fracture geometry), slurry rheology, and diffusion distance.

The model highlights the sensitivity of diffusion to key controllable parameters and serves as a guide for initial parameter selection. However, its predictions represent an upper bound. The findings of this study provide crucial complementary insights into slurry behavior relevant to mitigating clogging risks.

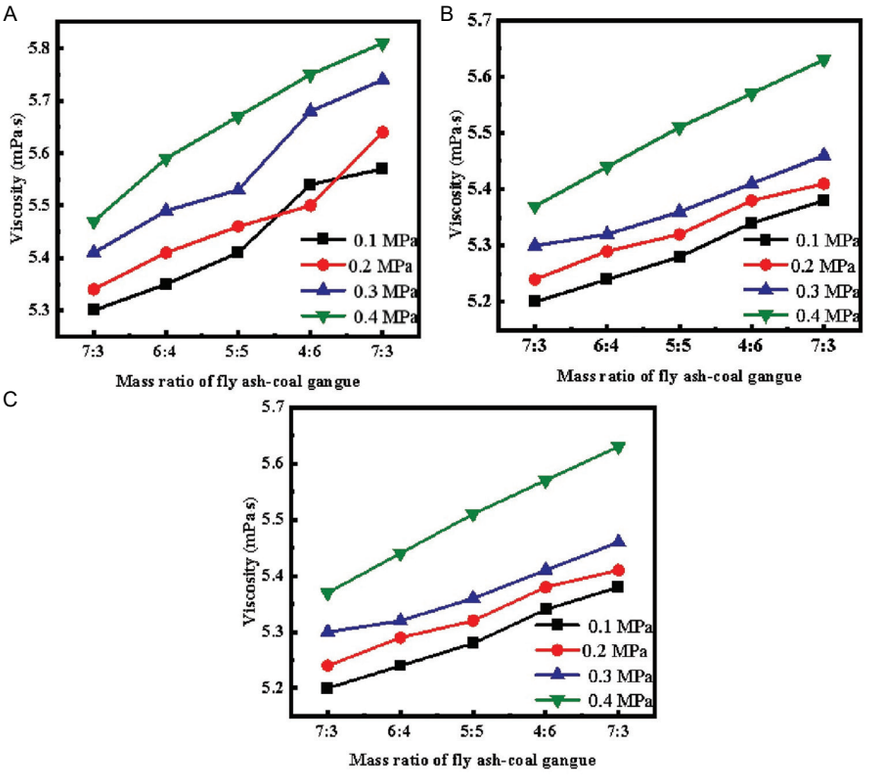

Figure 9. Slurry viscosity under injection pressure at varying fly ash-to-coal gangue mass ratios and coal gangue particle sizes: (A) 50 mesh, (B) 100 mesh, and (C) 150 mesh

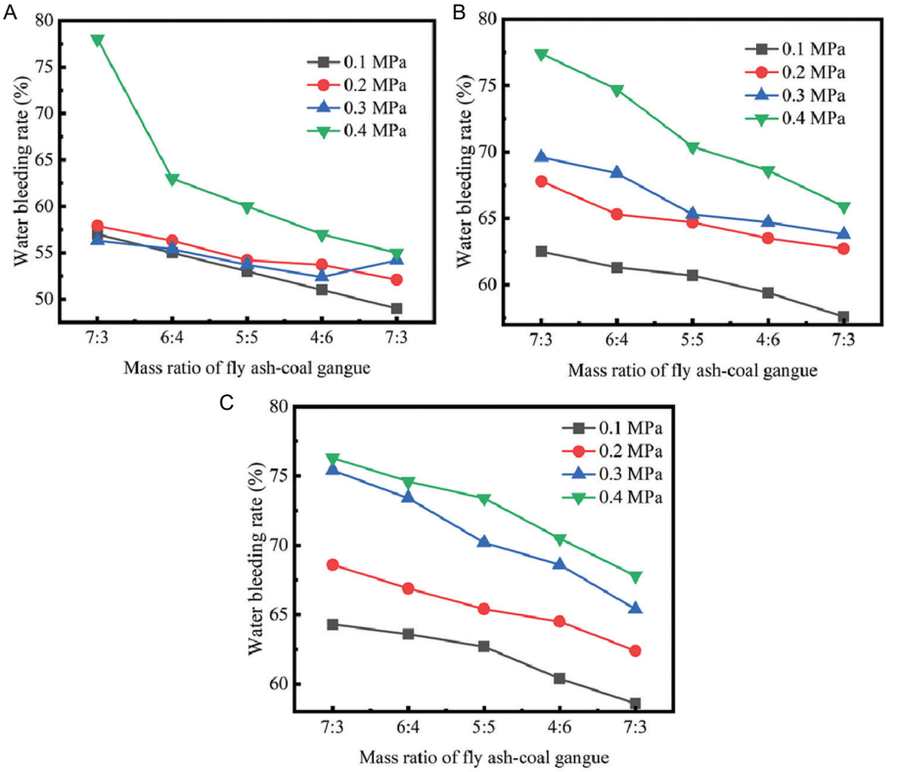

Figure 10. Water bleeding ratio of slurry under injection pressure at varying fly ash-to-coal gangue mass ratios and coal gangue particle sizes: (A) 50 mesh, (B) 100 mesh, and (C) 150 mesh

It is assumed that under injection pressure, the slurry is injected from the injection hole into the fracture and undergoes planar radial flow parallel to the fracture plane. The injection pressure at the injection hole is denoted as P_0, and the scouring force exerted by the water flow on the slurry is denoted as P_w.[33,34] A schematic diagram of the slurry diffusion in inclined fractures is shown in Figure 11. An arbitrary differential element is selected from Figure 11 for stress analysis, as illustrated in Figure 12. The formula for the power-law fluid fracture grouting diffusion model is presented in Equation I:

$$\begin{aligned}\left(\mathrm{P}+\mathrm{P_w}\right)\mathrm{r}\Delta\theta\Delta\mathrm{z}-\left[\left(\mathrm{P}+\mathrm{P_w}\right)+\frac{\mathrm{d}\left(\mathrm{P}+\mathrm{P_w}\right)}{\mathrm{dr}}\Delta\mathrm{r}\right]\left(\mathrm{r}+\Delta\mathrm{r}\right)\Delta\theta\Delta\mathrm{z}+\\ \left[\left(\mathrm{P}+\mathrm{P_w}\right)+\frac{\mathrm{d}\left(\mathrm{P}+\mathrm{P_w}\right)}{\mathrm{dr}}\frac{\Delta\mathrm{r}}{2}\right]\Delta\mathrm{r}\Delta\mathrm{z}\Delta\theta+\left(\frac{\mathrm{d}\tau}{\mathrm{dz}}\Delta\mathrm{z}\right)\\ \frac{\mathrm{r}\Delta\theta+\left(\mathrm{r}+\Delta\mathrm{r}\right)\Delta\theta}{2}\Delta\mathrm{r}+\rho\mathrm{g}\sin\alpha\Delta\mathrm{r}\Delta\mathrm{z}\\ \frac{\mathrm{r}\Delta\theta+\left(\mathrm{r}+\Delta\mathrm{r}\right)\Delta\theta}{2}=0\end{aligned} \tag{I}$$

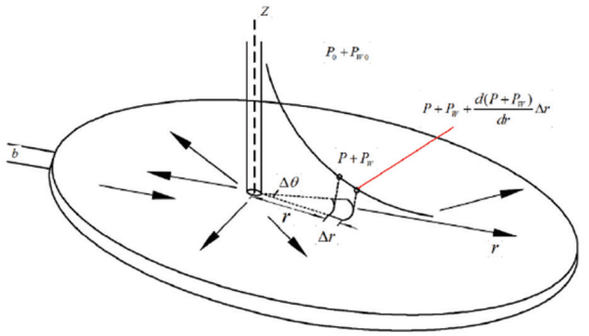

Figure 11. Schematic diagram illustrating slurry diffusion in inclined fractures

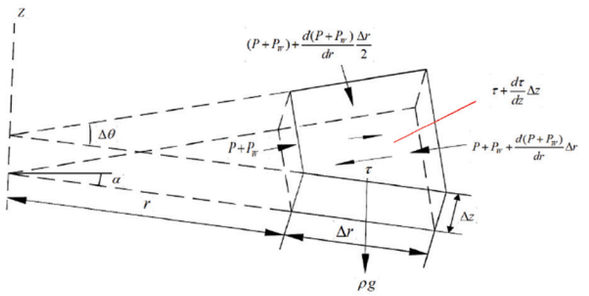

Figure 12. Stress analysis of a slurry element within an inclined fracture

Where:

(i) r represents the radius of the slurry spread (m).
(ii) Δr is the increment of the spread radius per unit time.
(iii) $\Delta\theta$ is the angle formed by the increment of the spread radius per unit time.
(iv) ρ is the density of the slurry (kg/m^3).
(v) α is the angle of the crack inclination; higher-order infinitesimal terms are neglected.

The equation can be simplified and organized as follows:

$$\frac{d\tau}{dz}=\frac{d\left(P+P_w\right)}{dr}-\rho g\sin\alpha \tag{II}$$

With respect to z, integration yields:

$$\tau=\left(\frac{d\left(P+P_w\right)}{dr}-\rho g\sin\alpha\right)\left(z+C_1\right) \tag{III}$$

Where C_1 is a constant determined by boundary conditions, which are then substituted into the equation.

$$\left.\frac{\mathrm{du}}{\mathrm{dz}}\right|_{z=0}=0\Rightarrow\mathrm{C_1}=0 \tag{IV}$$

$$\tau=\left(\frac{d\left(P+P_w\right)}{dr}-\rho g\sin\alpha\right)z \tag{V}$$

Additionally, the flow variation equation for a Newtonian fluid is generally expressed as:

$$\tau=k\left(\frac{du}{dz}\right)^n \tag{VI}$$

Substituting Equation VI into Equation V yields:

$$k\left(\frac{du}{dz}\right)^n=\left[\frac{d\left(P+P_w\right)}{dr}-\rho g\sin\alpha\right]z \tag{VII}$$

Integration with respect to z yields:

$$u=\frac{n}{n+1}\left[\frac{1}{k}\left(\frac{d\left(P+P_w\right)}{dr}-\rho g\sin\alpha\right)\right]^{\frac{1}{n}}\left(z^{\frac{n+1}{n}}+C_2\right) \tag{VIII}$$

Based on the boundary conditions:

$$\left.u\right|_{z=\pm\frac{b}{2}}=0\Rightarrow C_2=-\left(\frac{b}{2}\right)^{\frac{n+1}{n}} \tag{IX}$$

$$u=\frac{n}{n+1}\left[\frac{1}{k}\left(\frac{d\left(P+P_w\right)}{dr}-\rho g\sin\alpha\right)\right]^{\frac{1}{n}}\left(z^{\frac{n+1}{n}}-\left(\frac{b}{2}\right)^{\frac{n+1}{n}}\right) \quad \text{(X)}$$

In this equation, b represents the fracture opening (m). The average flow velocity of the slurry is:

$$\bar{u}=\frac{1}{b}\int_{-\frac{b}{2}}^{\frac{b}{2}}\frac{n}{n+1}\left[\frac{1}{k}\left(\frac{d\left(P+P_w\right)}{dr}-\rho g\sin\alpha\right)\right]^{\frac{1}{n}}\left(z^{\frac{n+1}{n}}-\left(\frac{b}{2}\right)^{\frac{n+1}{n}}\right)$$

$$dz=\frac{-n}{2n+1}\left[\frac{1}{k}\left(\frac{d\left(P+P_w\right)}{dr}-\rho g\sin\alpha\right)\right]^{\frac{1}{n}}\left(\frac{b}{2}\right)^{\frac{n+1}{n}} \quad \text{(XI)}$$

Assuming that the slurry spreads in a semicircular pattern along the direction of water flow, the unit flow rate of the slurry is given by:

$$q=\pi rb\bar{u}=\pi rb\frac{-n}{2n+1}\left(\frac{b}{2}\right)^{\frac{n+1}{n}}\left[\frac{1}{k}\left(\frac{d\left(P+P_w\right)}{dr}-\rho g\sin\alpha\right)\right]^{\frac{1}{n}} \quad \text{(XII)}$$

In this equation, q represents the slurry flow rate, while r represents the spread radius (m).

Integration with respect to r yields:

$$P+P_w=\begin{cases}\rho g\sin\alpha r-\dfrac{kq^n}{\left(1-n\right)\pi^n b^n\left(\dfrac{n}{2n+1}\right)^n\left(\dfrac{b}{2}\right)^{n+1}}r^{1-n}+C_3,\ n\neq 1\\ \rho g\sin\alpha r-\dfrac{12kq}{\pi b^3}\ln r+C_3,\quad n=1\end{cases} \quad \text{(XIII)}$$

Based on the boundary conditions ($r = r_0$; $P = P_0$; $P_w = P_{w0}$), C_3 can be obtained using the following equation:

$$C_3=\begin{cases}P_0+P_{w0}-\rho g\sin\alpha r_0\\ +\dfrac{kq^n}{\left(1-n\right)\pi^n b^n\left(\dfrac{n}{2n+1}\right)^n\left(\dfrac{b}{2}\right)^{n+1}}r_0^{1-n},\quad n\neq 1\\ P_0+P_{w0}-\rho g\sin\alpha r_0+\dfrac{12kq}{\pi b^3}\ln r_0,\quad n=1\end{cases} \quad \text{(XIV)}$$

Where P_{w0} represents the hydrodynamic force exerted by the water flow on the slurry at the grouting hole (Pa), while r_0 denotes the radius of the grouting hole (m).

$$P+P_w=\begin{cases}P_0+P_{w0}+\rho g\sin\alpha\left(r-r_0\right)\\ -\dfrac{kq^n}{\left(1-n\right)\pi^n b^n\left(\dfrac{n}{2n+1}\right)^n\left(\dfrac{b}{2}\right)^{n+1}}\left(r^{1-n}-r_0^{1-n}\right),n\neq 1\\ P_0+P_{w0}+\rho g\sin\alpha\left(r-r_0\right)-\dfrac{12kq}{\pi b^3}\ln\dfrac{r}{r_0},\quad n=1\end{cases} \quad \text{(XV)}$$

The injection volume per unit time corresponds to the volume of slurry required to extend the spread radius during that time interval:

$$\int_0^t q\,dt=\int_{r_0}^{r}\pi rb\,dr \quad \text{(XVI)}$$

Where t represents the grouting time (s).

$$qt=\frac{\pi b}{2}\left(r^2-r_0^2\right) \quad \text{(XVII)}$$

Substituting Equation VI into Equation XIII yields $P + P_w$ when $n \neq 1$:

$$P+P_w=P_0+P_{w0}+\rho g\sin\alpha\left(r-r_0\right)-\frac{2k\left(r^2-r_0^2\right)^n}{\left(1-n\right)b^{n+1}\left(\dfrac{n}{2n+1}\right)^n t^n\left(r^{1-n}-r_0^{1-n}\right)}\left(1-n\right)\pi b^n \quad \text{(XVIII)}$$

$$P+P_w=P_0+P_{w0}+\rho g\sin\alpha\left(r-r_0\right)-\frac{6k\left(r^2-r_0^2\right)}{b^2t}\ln\frac{r}{r_0}\,n=1 \quad \text{(XIX)}$$

Under static water conditions, the boundary conditions at the maximum spread radius of the slurry are: $r = r_{max}$, $P = 0$, $P_w = P_c$. By substituting the boundary conditions, the following expression is obtained:

$$P_c=P_0+P_{w0}+\rho g\sin\alpha\left(r_{max}-r_0\right)-\frac{6k\left(r_{max}^2-r_0^2\right)}{b^2t}\ln\frac{r_{max}}{r_0}\,n=1 \quad \text{(XX)}$$

In the equation, P_c represents the hydrostatic pressure (Pa).

$$P_c=P_0+P_{w0}+\rho g\sin\alpha\left(r_{max}-r_0\right)-\frac{2k\left(r_{max}^2-r_0^2\right)^n}{\left(1-n\right)b^{n+1}\left(\dfrac{n}{2n+1}\right)^n t^n}\left(r_{max}^{1-n}-r_0^{1-n}\right)n\neq 1 \quad \text{(XXI)}$$

Accordingly, the relationship between the diffusion distance of the slurry against the slurry flow direction and the injection time is expressed as:

$$t = \frac{6\eta}{b^2\left(P_0 - \frac{1}{2}\rho_w v^2 - P_c\right)}\left(r^2 \ln\left(\frac{r}{r_0}\right) - \frac{r^2 - r_0^2}{2}\right) \quad \text{(XXII)}$$

To investigate the influence of grouting pressure, fracture width, and fracture inclination angle on grout diffusion distance, the following parameters were adopted: Rheological index ($n = 0$), hydrostatic pressure (0.1 MPa), P_c (0.1 MPa), slurry density (13.40 kN/m^3), gravimetric density of coal gangue, γg (13.40 kN/m^3), and injection hole radius ($r_0 = 60$ mm).[34,35] The injection pressure (P_0 = 0.1–0.4 MPa), crack width (b = 0.4–1.0 mm), and fracture inclination angle (α = 5–20°) were varied. The relationship between grouting time and grout diffusion distance under varying grouting pressures, fracture widths, and fracture inclination angles was calculated using Equation XXII and illustrated in Figure 13.

As injection pressure increases, the diffusion distance progressively expands. Higher injection pressures result in greater diffusion distances. In practice, elevated injection pressure promotes fracture dilation, thereby widening the flow channels and enhancing the integration of the injected slurry with fractured rock masses.

As injection time increases, the slope of the curves under all pressure conditions gradually decreases, indicating that the time required to reach the ultimate diffusion distance also increases with higher injecting pressures. During initial injection, low-pressure injection is recommended to prevent excessive spread beyond the design range. Subsequently, high-pressure fracture grouting should be applied to achieve the dilation and filling of closed or slightly open fractures.[14]

When injection time is held constant, larger fracture widths correspond to greater diffusion distances. Thus, fracture width is directly proportional to diffusion distance–wider fractures yield longer diffusion distances. However, as fracture width increases, the time required to achieve the ultimate diffusion distance also lengthens. Fracture inclination angle is also directly proportional to grout diffusion distance—steeper angles lead to longer diffusion distances.[33] However, as the inclination angle increases, the rate of increase in diffusion distance over the same duration exhibits a declining trend.

Several limitations remain in this study, including the exclusion of fracture permeability variations and particle

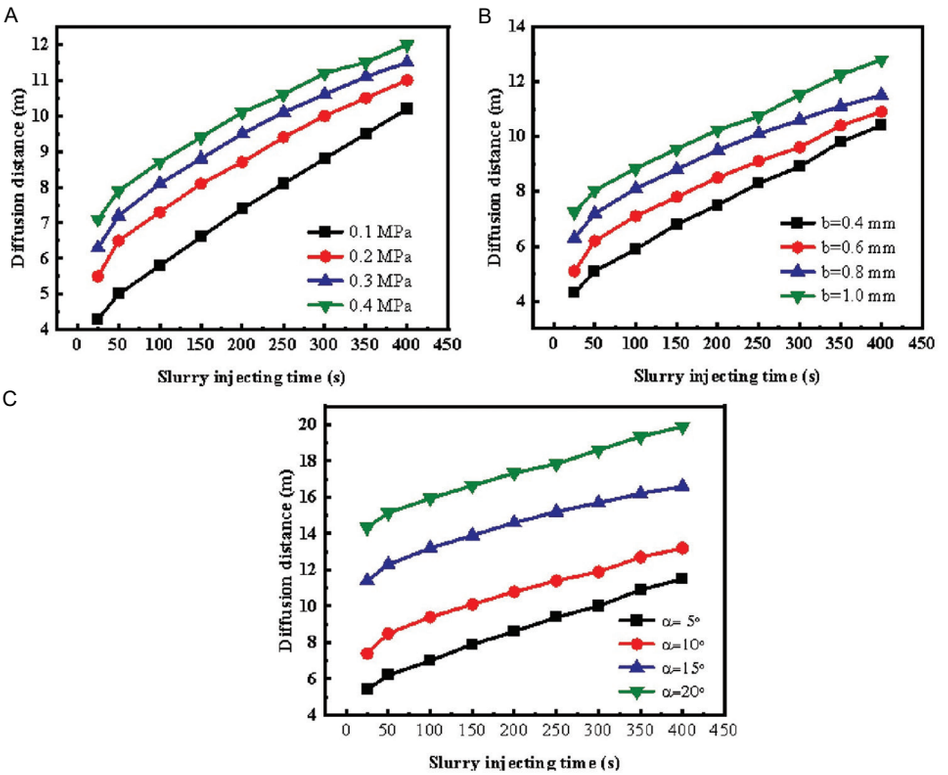

Figure 13. Predicted slurry diffusion distance under varying (A) injection pressures, (B) fracture widths, and (C) fracture inclination angles

filtration effects. Moreover, bleeding behavior requires validation under field-simulated strata conditions, and long-term geochemical stability beyond the 12-h test period was not evaluated.

4. Conclusion

This study examined the feasibility of utilizing coal gangue–fly ash slurry as a filling material for grouting in separated-bed technology. The main findings are summarized as follows:

(i) The variations in solid volume concentration, coal gangue particle size, and fly ash-to-coal gangue mass ratio exerted significant effects on slurry density, with approximately linear relationships observed. All three factors showed statistically significant differences ($p<0.01$) in their effects on viscosity, with the order of influence ranked as: solid volume concentration > coal gangue particle size > fly ash-to-coal gangue mass ratio.

(ii) The slurry viscosity increased progressively with higher coal gangue mass proportions. Notably, when the coal gangue proportion reached 70%, the viscosity increased sharply. This effect is attributed to the larger particle size of coal gangue compared to fly ash, which amplifies internal friction and hinders particle mobility, thereby leading to higher viscosity.

(iii) Solid volume concentration and the fly ash-to-coal gangue mass ratio were the primary factors influencing the water bleeding rate. Changes in water bleeding behavior varied across different stages of coal gangue mass proportion due to the larger interstitial voids associated with coal gangue particles, which require filling by either fly ash or water. Variations in mass proportion altered the distribution of interstitial water and fly ash, leading to differential water bleeding behaviors.

(iv) Polycarboxylate superplasticizer significantly reduced slurry viscosity, with viscosity progressively decreasing as superplasticizer dosage increased. The long polymer chains of polycarboxylate physically separated the particles, preventing agglomeration and significantly reducing interparticle friction. In contrast, sulfamic acid primarily generated weaker electrostatic repulsion, which was insufficient for complete particle dispersion.

(v) Higher grouting pressure increased the water bleeding rate and shortened the time required to complete bleeding. Finer coal gangue particle sizes reduced the bleeding rate, while a higher coal gangue content also contributed to a lower water bleeding ratio in the slurry.

(vi) The power-law fluid model predicted that diffusion distance increased with injection pressure (0.1–0.4 MPa) and fracture width (0.4–1.0 mm), while steeper fracture angles (up to 20°) enhanced slurry spread but with diminishing incremental effects. Implementing low-pressure initial grouting followed by staged pressure increases helps minimize unintended spread and improves fracture filling efficiency.

Acknowledgments

None.

Funding

This research was funded by the Science and Technology Project of the Guizhou Provincial Energy Bureau (Project title: Technical Research and Development of Coal Gangue Underground Backfill Mining Technology and Pilot Application, undertaken by Guizhou Zhaping Coal Industry Co., Ltd.) (Grant number: 2023–68).

Conflict of interest

The authors declare that they have no competing interests.

Author contributions

Conceptualization: Jian Wang, Linqiang Mao
Formal analysis: Xiao Wang
Funding acquisition: Jian Wang
Investigation: Zhu Liu, Shupeng Wen
Methodology: Jian Wang, Yang Yang, Zhongquan Liu
Writing–original draft: Zhu Liu, Shupeng Wen
Writing–review & editing: Linqiang Mao

Availability of data

Data is available from the corresponding author upon reasonable request.

References

1. Zhang LM, Lai XP, Pan JL, *et al*. Experimental investigation on the mixture optimization and failure mechanism of cemented backfill with coal gangue and fly ash. *Powder Technol*. 2024;440:119751. doi: 10.1016/j.powtec.2024.119751

2. Shi Y, Gan L, Li XB, He SY, Sun C, Gao L. Dynamics of metals in backfill of a phosphate mine of guiyang, China using a three-step sequential extraction technique. *Chemosphere*. 2018;192:354-361. doi: 10.1016/j.chemosphere.2017.10.161
3. Zhang SY, Zhao YL, Zhang XQ, Wang K. Durability and heavy metals leaching behavior of cemented paste backfill using chemical activated binary slag as binder under sulfate attack. *Case Stud Constr Mater*. 2024;20:e03065. doi: 10.1016/j.cscm.2024.e03065
4. Švajlenka J, Pošiváková T, Hermawan H. User perspectives on sustainable innovation in the construction industry. *Asian J Water Environ*. 2025;22:211-220. doi: 10.36922/AJWEP025080047
5. Long K, Li B, Ma J, Liu H, Li J. Ecological risk analysis of leakage caused by coal-based solid waste backfill slurry bleeding: An experimental study. *J Clean Prod*. 2025;494:144993. doi: 10.1016/j.jclepro.2025.144993
6. Yao YN, El Naggar MH, Zhang J, Xu J, Yang J, Li M. Dynamic mechanical properties of coal-based solid waste cemented backfill material. *J Build Eng*. 2024;98:111347. doi: 10.1016/j.jobe.2024.111347
7. Yang B, Zheng Z, Jin J, Wang X. Time-dependent rheological properties of cemented aeolian sand-fly ash backfill vary with particles size and plasticizer. *Materials*. 2023;16:5295. doi: 10.3390/ma16155295
8. Cheng QQ, Wang HD, Guo YB, *et al*. Experimental study on mechanical properties of coal-based solid waste nanocomposite fiber cementitious backfill material. *Materials (Basel)*. 2023;16:5314. doi: 10.3390/ma16155314
9. Wang HS, Chen DF, Guo RH, Tian JH, Li B. A preliminary study on the improvement of gangue/tailing cemented fill by bentonite: Flow properties, mechanical properties and permeability. *Materials (Basel)*. 2023;16:6802. doi: 10.3390/ma16206802
10. Wang X, Zhang JX, Li M, *et al*. Expansion properties of cemented foam backfill utilizing coal gangue and fly ash. *Minerals*. 2022;12:763. doi: 10.3390/min12060763
11. Zheng Z, Yang B, Gu C, Yang F, Liu H. Experimental investigation into the proportion of cemented aeolian sand-coal gangue-fly ash backfill on mechanical and rheological properties. *Minerals*. 2023;13:1463. doi: 10.3390/min13111436
12. Zhang Y, Zhou W, Li M, Chen Z. Experimental study on compression deformation and permeability characteristics of grading broken gangue under stress. *Processes*. 2018;6:257. doi: 10.3390/pr6120257
13. Zhang Y, Baaj H, Zhao R. Evaluation for the leaching of Cr from coal gangue using expansive soils. *Processes*. 2019;7:478. doi: 10.3390/pr7080478
14. Wang Y, Huang Y, Hao Y. Experimental study and application of rheological properties of coal gangue-fly ash backfill slurry. *Processes*. 2020;8:284. doi: 10.3390/pr8030284
15. Ju F, Li B, Guo S, Xiao M. Dynamic characteristics of gangues during vertical feeding in solid backfill mining: A case study of the Wugou coal mine in China. *Environ Earth Sci*. 2016;75:1389. doi: 10.1007/s12665-016-6194-0
16. Bo L, Yang SQ, Liu Y, Zhang ZH, Wang YY, Wang YW. Coal mine solid waste backfill process in China: Current status and challenges. *Sustainability*. 2023;15:13489. doi: 10.3390/su151813489
17. Du ZW, Chen DY, Li XL, *et al*. Study on the partial paste backfill mining method in a fully mechanized top-coal caving face: Case study from a coal mine, China. *Sustainability*. 2024;16:4393. doi: 10.3390/su16114393
18. Wang JX, Xing MH, Yang XL, *et al*. Study on the long-term durability and leaching characteristics of low-consumption cement backfill under different environmental conditions. *Sustainability*. 2024;16:5138. doi: 10.3390/su16125138
19. Li W, Yue L, Liu Y, Li SC, Ma LQ, Wang JT. Study on mechanical properties of coal gangue and fly ash mixture as backfill material based on fractal characteristics. *Environ Sci Pollut Res*. 2023;30:111936-111946. doi: 10.1007/s11356-023-30221-4
20. Shi P, Zhang J, Yan H, *et al*. Mechanical properties evaluation of waste gangue-based cemented backfill materials based on an improved response surface model. *Environ Sci Pollut Res Int*. 2024;31:3076-3089. doi: 10.1007/s11356-023-31368-w
21. Yin YC, Zou JC, Zhang YB, Qiu Y, Fang K, Huang DM. Experimental study of the movement of backfilling gangues for goaf in steeply inclined coal seams. *Arab J Geosci*. 2018;11:318. doi: 10.1007/s12517-018-3686-0
22. Wang CX, Shen BT, Chen JT, *et al*. Compression characteristics of filling gangue and simulation of mining with gangue backfilling: An experimental investigation. *Geomech Eng*. 2020;20:485-495. doi: 10.12989/gae.2020.20.6.485
23. Gu WZ, Yang BG, Pan H, Song TQ. Research and engineering practice on space characteristics of gangue slurry filling. *Sci Rep.* 2023;13:22006. doi: 10.1038/s41598-023-46222-9
24. Zhou N, Zhang JX, Xu JF, *et al*. Experimental study on the flow and diffusion laws of heterogeneous gangue slurry in mining space. *Rock Mech Rock Eng*. 2025;58:2589-2605. doi: 10.1007/s00603-024-04367-7
25. Wang JQ, Zhang Q, Yin W, Qi SM, Gao DF, Ma D.

On-site measurement on compaction characteristics of coal gangue and surface subsidence disaster in deep backfilling mining. *Front Earth Sci*. 2021;9:724476. doi: 10.3389/feart.2021.724476
26. Tai Y, Guo S, Lan LX. Reasonable gangue section length for disposing gangue pollutants in the new green mixed workface. *Bull Eng Geol Environ*. 2019;79:1669-1682. doi: 10.1007/s10064-019-01677-x
27. Sun Q, Tian S, Sun Q, *et al*. Preparation and microstructure of fly ash geopolymer paste backfill material. *J Clean Prod*. 2019;225:376-390. doi: 10.1016/j.jclepro.2019.03.310
28. Wang QP, Zhu LT, Lu CY, Liu YX, Yu QB, Chen S. Investigation on the effect of calcium on the properties of geopolymer prepared from uncalcined coal gangue. *Polymers (Basel)*. 2023;15:1241. doi: 10.3390/polym15051241
29. Li M, Zhang J, Li A, Zhou N. Reutilisation of coal gangue and fly ash as underground backfill materials for surface subsidence control. *J Clean Prod*. 2020;254:120113. doi: 10.1016/j.jclepro.2020.120113
30. Dou G, Wang C, Zhong X, Qin B. Preparation and characterization of green lignin modified mineral cementitious firefighting materials based on uncalcined coal gangue and coal fly ash. *Constr Build Mater*. 2024;435:136799. doi: 10.1016/j.conbuildmat.2024.136799
31. Sun JK, Zhou CC, Shen HX, *et al*. Green synthesis of ceramsite from industrial wastes and its application in selective adsorption: Performance and mechanism. *Environ Res*. 2022;214:113786. doi: 10.1016/j.envres.2022.113786
32. Yang J, Su Y, He XY, *et al*. Pore structure evaluation of cementing composites blended with coal by-products: Calcined coal gangue and coal fly ash. *Fuel Process Technol*. 2018;181:75-90. doi: 10.1016/j.fuproc.2018.09.013
33. Bui DH, Nghiem XH. The effects of urbanization on air pollution and public health in Vietnam: An empirical analysis. *Asian J Water Environ*. 2025;22:198-210. doi: 10.36922/AJWEP025130088
34. Mounira C. Sustainable wastewater management and risk assessment in Maghnia. *Asian J Water Environ*. 2025;22:164-184. doi: 10.36922/AJWEP025120085
35. Hu Y, Liu W, Shen Z, Gao K, Liang D, Cheng S. Diffusion mechanism and sensitivity analysis of slurry while grouting in fractured aquifer with horizontal injection hole. *Carbonate Evaporite*. 2020;35(2):1-16. doi: 10.1007/s13146-020-00587-4